

## CALIBRATION OF ELECTROMAGNETIC CALORIMETERS IN HIGH ENERGY EXPERIMENTS WITH A RADIO FREQUENCY QUADRUPOLE ACCELERATOR<sup>+</sup>

H. MA, H. NEWMAN and R.Y. ZHU

*California Institute of Technology, Pasadena, CA 91125, USA*

R. HAMM

*AccSys Technology, Inc., Pleasanton, CA 94566, USA*

Received 10 March 1989

A fast, effective calibration technique has been developed for future Superconducting Supercollider (SSC) calorimeters based upon the radiative capture of protons from a pulsed Radio Frequency Quadrupole (RFQ) accelerator in a fluoride target. The intense flux of low energy photons acts as a clean “pulse generator” calibration signal equivalent to 20 GeV or more. This calibration technique has been demonstrated with a bismuth germanate (BGO) detector array, as well as with several barium fluoride detector crystals, to provide a calibration accuracy of 0.5% within two minutes. The SSC calibration has resulted from the development of this novel technique by Caltech over the past five years for the L3 BGO electromagnetic calorimeter, which uses a lithium target for the production of 17.6 MeV low energy photons for the calibration source. Proven techniques have been developed to provide an in situ calibration for all 11 000 BGO detector crystals, with an accuracy of 0.8% obtainable in 1–2 h. The result of the experimental test by using the AccSys RFQ accelerator is reported, as is the preliminary concept of a small storage ring that can be used to compress the output beam pulse from the RFQ accelerator into a target beam pulse of 100 ns or less.

### 1. Introduction

The high luminosity and high center of mass energy available at future accelerators, such as the Superconducting Supercollider (SSC) and the Large Hadronic Collider (LHC), have presented a great challenge to HEP experimentalists faced with the problem of detector design [1].

Rapid and precise calibrations in situ have always been essential to maintain the design performance of high resolution calorimeters. This will be particularly true in the case of detectors at the SSC and LHC, where high radiation doses may cause rapid gain shifts in individual calorimeter elements, especially near the beam line [2]. Many present-day calibration techniques, such as the use of radioactive sources and cosmic rays, would no longer work at these accelerators because the deposited energy in a calorimeter element will, in most cases, fall below the lower limit of the dynamic range (GeV to TeV) of the readout electronics. The time to accumulate sufficient statistics for a precise calibration,

for future calorimeters with  $10^4$  elements or more, also would be prohibitive.

Over the last five years, the Caltech group has developed and tested a novel calibration technique [3,4] based on the radiative capture of a pulsed proton beam from a Radio Frequency Quadrupole (RFQ) accelerator in a lithium target,  ${}^7\text{Li}(p, \gamma){}^8\text{Be}$ . The resultant high intensity flux of 17.6 MeV photons can be used to calibrate the thousands of bismuth germanate (BGO) crystals in the L3 electromagnetic calorimeter at once, with an absolute accuracy of better than 1% in 1–2 h. When installed in the L3 experiment at LEP, this system will help ensure that the high resolution of the electromagnetic calorimeter is maintained during running. This experience culminated in a test of a BGO crystal array at the RFQ facility at AccSys Technology, Inc. in Pleasanton, California in November, 1987. An absolute calibration precision of better than 1% was achieved in the test [4].

Following the 1987 test, we realized the possibility of a new technique, appropriate for the calibration of calorimeters at the SSC or other accelerators in the TeV range. By using the radiative capture of protons from a pulsed beam in a fluoride target,  ${}^{19}\text{F}(p, \alpha){}^{16}\text{O}^*$  [5], and the subsequent decay of the excited oxygen nucleus,  ${}^{16}\text{O}^*$ , hundreds to thousands of 6 MeV photons could be produced per milliradian per pulse. These “equiv-

<sup>+</sup> Work supported in part by US Department of Energy Contracts no. DE-AC03-88-ER80674 and DE-AC03-81-ER40050.

alent high energy photons" would serve as a calibration source for electromagnetic calorimeters.

A milestone beam test was carried out in September, 1988 at AccSys under a Phase I grant from the DoE Small Business Innovative Research (SBIR) program, where four BaF<sub>2</sub> counters were set up together with a 7 × 7 L3 BGO crystal array as a reference counter. The test demonstrated that this technique functions as a clean "pulse generator" of scintillation light, originating several cm inside the crystals. The clean, narrow Gaussian-distributed light pulses produced with this technique were shown to provide relative calibrations with a precision of 0.5% or better in a few minutes.

This report describes the RFQ-based calibration and summarizes the results of the test. The next section describes the RFQ, the detector setup and the running conditions of the test. The results of the test are presented in the third section. A summary, and the outlook for future RFQ tests with a BaF<sub>2</sub> crystal array are given in the last section.

## 2. Accelerator and experimental setup

### 2.1. RFQ system

The AccSys RFQ uses an H<sup>+</sup> ion source and produces a 1.92 MeV pulsed proton beam. A detailed description of the RFQ system can be found in our previous report, on calibration tests for the L3 BGO electromagnetic calorimeter [4]. To obtain a high photon flux per pulse, the run parameters of the AccSys RFQ were adjusted for this test as follows:

- pulse width: 8 μs full width at half-height (10 μs at the base);
- peak current: adjustable, up to 24 mA;
- pulse repetition rate: adjustable, up to 30 Hz.

Fig. 1 shows a typical RFQ beam pulse together with the gate signal applied to the LeCroy 2249W ADC which was used to read out the pulse.

The proton beam was bent by a dipole magnet by 22.5°. A pair of small permanent quadrupole magnets was installed to focus the beam spot onto the target with a diameter that could be adjusted, down to a few millimeters.

### 2.2. Target

Proton capture in a fluorine nucleus, <sup>19</sup>F(p, α)<sup>16</sup>O\*, and the subsequent radiative decay of the excited oxygen

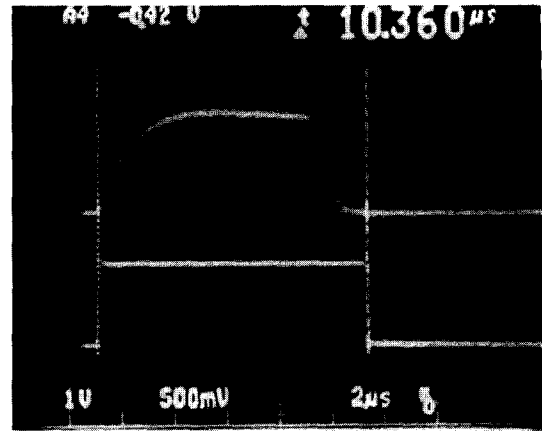


Fig. 1. RFQ beam pulse and integration gate.

nucleus, <sup>16</sup>O\*, were used to produce photons. The yield of photons was sufficient to deposit up to several GeV in a single crystal covering a solid angle of 1.6 msr. This corresponded to the typical case for an L3 BGO crystal, with a 2 × 2 cm<sup>2</sup> front face situated at a distance of 50 cm from the LEP interaction point.

LiF was used as the target material. The LiF crystals were encapsulated in a molybdenum holder, with a 0.9 cm diameter thin foil facing the beam. Three target foils were tested: 5 μm thick molybdenum, 10 μm molybdenum, or 5 μm gold. Molybdenum was chosen as the preferred foil and holder material because of its high melting point, mechanical strength and low photon background (tested in earlier tests at Los Alamos and at the Caltech Kellogg Van de Graaff) when bombarded with a proton beam.

The foils were designed to help conduct heat away from the fluoride target and to prevent the proton beam from hitting the <sup>7</sup>Li neutron resonance which has a threshold of 1.88 MeV, since the energy of AccSys RFQ is 1.92 MeV. The foils also served as an energy degrader for the proton beam. Since the energies of the protons hitting the target differed for different target thickness, the dependence of the photon yield per beam pulse on the proton energy could be measured.

Table 1 lists the sizes of the three LiF crystals used as targets and the foils used. The energy of the proton beam ( $E_p$ ) hitting the crystals, after penetrating the foil, is also shown in the table.

The targets were mounted in a vacuum glass tee on movable shafts connected through an O-ring assembly

Table 1  
LiF targets, Mo and Au foils

Size	10 mm(diameter) × 1 mm	10 mm(diameter) × 1 mm	12 mm(diameter) × 1 mm
Foil	5 μm Mo	10 μm Mo	5 μm Au
$E_p$	1.6 MeV	1.2 MeV	1.5 MeV

to the outside. This allowed us to adjust the target position, or to pull one target out and put another target in without interrupting the RFQ operation. The target and mounting shaft were electrically connected to ground through a 100  $\Omega$  resistor. The voltage across the resistor was inverted and attenuated, then fed into a LeCroy 2249W ADC to measure the integrated beam charge per pulse.

The target with a 5  $\mu\text{m}$  Mo foil in front was tested up to 20 W average beam power during a test at the Kellogg Van de Graaff facility at Caltech in the Summer of 1988. At AccSys two Mo targets survived the beam test with up to 8 W average power. The gold foil, however, was unable to withstand the heat deposited in a small spot by the beam and was punctured. Therefore, the target with the damaged gold foil was considered as a bare target. As described below, this had important consequences for the test results.

### 2.3. BGO crystal matrix

A  $7 \times 7$  matrix of L3 standard size BGO crystals, approximately 2 cm  $\times$  2 cm in the front, 3 cm  $\times$  3 cm in the back and 24 cm long, was assembled in a 0.2 mm thick carbon fiber structure. All of the crystals were produced at the Shanghai Institute of Ceramics, Shanghai, China. The crystals were polished and painted with NE560 white paint to provide a high light yield and good light collection uniformity, using methods similar to those developed by the L3 Collaboration at CERN.

The complete structure was installed in an aluminum box with air cooling provided by a refrigerator. Twenty temperature sensors were installed inside the BGO matrix, including small sensors inserted between the crystals, to monitor the temperature variations throughout the series of runs, and to allow us to correct the gain for each crystal to sufficient accuracy off-line. The temperature of the BGO crystals was kept at about 22°C with less than 2°C variation from run to run, while the environmental temperature in the AccSys assembly hall where the tests were carried out varied from 25°C to 40°C.

The BGO matrix was read out using the same Hamamatsu photodiodes, Lyon preamplifiers, and Princeton digitization boards used in the L3 experiment [8]. A Motorola 68020 CPU-based single board computer running at 20 MHz was used to control a token-passing ring of ADC boards, and to communicate with a VAXStation II computer through a home-made CAMAC FIFO module. A more detailed description of the readout system can be found in our previous publication [4].

The synchronized trigger provided by the RFQ control electronics was used to start the data-taking time sequence in a homemade interface board built at

Caltech. The time chain provided reset, sample/hold and interrupt signals for the microprocessor-controlled ADC boards. The integration time was adjusted to 15  $\mu\text{s}$  to cover the typical 10  $\mu\text{s}$  beam pulse width plus 5  $\mu\text{s}$ , so that the charge pulse read out from each BGO crystal was fully integrated. (The scintillation light from BGO has a 300 ns characteristic decay time). Although the data acquisition system was capable of handling a trigger rate of more than 150 Hz, we were limited by the available RFQ power supply setup to a maximum beam pulse repetition rate of 30 Hz, for high current pulses.

The electronic gains of the slow dc amplifiers, and the pedestal (offset) of the high energy-range channel on each dual-range ADC board, were calibrated at Caltech by using a test pulse. The complete BGO matrix was calibrated at AccSys with runs using a metallic lithium target, prior to the tests with the fluoride targets. The gain of each crystal was determined in this first round of runs from the position in the energy spectrum corresponding to the half-height of the front edge, called "HH<sup>+</sup>", following the techniques developed in our 1987 AccSys test [4]. The calibration point was thus determined to an absolute accuracy of 0.8%.

### 2.4. BaF<sub>2</sub> detector

BaF<sub>2</sub> is a unique high density inorganic scintillator with three emission spectra peaking at 195, 220 and 310 nm, with decay time constants of 0.87, 0.88 and 600 ns, respectively [6]. Because of the speed of the "short" or "fast" components and the compelling evidence that it has high radiation resistance [7], BaF<sub>2</sub> has been considered to be one of the most promising candidate materials for future electromagnetic calorimeters.

Four BaF<sub>2</sub> counters were constructed for this test. The crystals were obtained from Harshaw (USA), OKEN (Ohyo-Koken in Japan) and Merck (E. Merck, Darmstadt, FRG). Table 2 lists the sizes and manufacturers of the crystals, and the photomultipliers (PMTs) attached to them.

The BaF<sub>2</sub> crystals were polished and wrapped with two layers of teflon tape. Hamamatsu R2078 and R3197 PMTs were chosen to read out the fast components of the scintillation pulse, while a Hamamatsu R1306 PMT was chosen to read out the slow component. The R3197 and R2078 tubes both have synthetic silica (quartz)

Table 2  
BaF<sub>2</sub> crystals and photomultipliers

	Manufacturer	Size	PMT	Sensitivity
1	Harshaw	2 in. (diameter) $\times$ 3 in.	R1306	slow
2	Oken	47 mm $\times$ 47 mm $\times$ 67 mm	R3197	fast
3	Merck	3 in. (diameter) $\times$ 3 in.	R1306	slow
4	Harshaw	1 in. (diameter) $\times$ 1 in.	R2078	fast

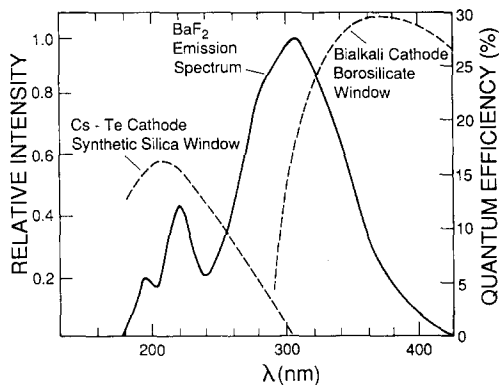


Fig. 2. BaF<sub>2</sub> scintillation spectrum and PMT response.

windows and Cs–Te photocathodes. The quartz window has greater than 80% transmittance for wavelengths longer than 180 nm. The Cs–Te photocathodes are mainly sensitive only to wavelengths between 160 and 300 nm, i.e. they are UV-sensitive and solar-blind. The quantum efficiencies of the R2078 and R3197 at 200 nm, which is near the peak of the fast component of the BaF<sub>2</sub> spectrum, are 18% and 13% respectively. Fig. 2 shows the scintillation spectrum of BaF<sub>2</sub> and the quantum efficiency of a typical Cs–Te photocathode with a quartz window. The fast to slow ratio in the R3197 or R2078 PMT output is approximately 1:2 with full integration. The fast component can then be separated out by using a short gate to integrate the collected charge.

The R1306 PMT has a borosilicate glass window and a conventional bialkali photocathode. The quantum efficiency of this photocathode and window combination is also shown in fig. 2.

The PMTs were coupled to the crystals with Dow Corning 200 fluid, with a viscosity of 12 500 cp, which has good UV transmittance. The output of the PMTs was integrated and digitized by using a LeCroy 2249W ADC CAMAC module.

All BaF<sub>2</sub> counters were tested at Caltech before the AccSys test with a <sup>137</sup>Cs source. A typical resolution of 11% (FWHM) was obtained with an R1306 PMT for the fast plus slow components, and 47% (FWHM) with an R3197 PMT for the fast component with a 50 ns integration time. Fig. 3 shows the pulse height spectra obtained with a <sup>137</sup>Cs source from the BaF<sub>2</sub> counters.

### 2.5. Running conditions

Fig. 4 shows a schematic view of the detector setup, together with the RFQ accelerator and the target at AccSys. The BGO matrix and the BaF<sub>2</sub> counters were placed 52 cm away from the target, as shown in the figure.

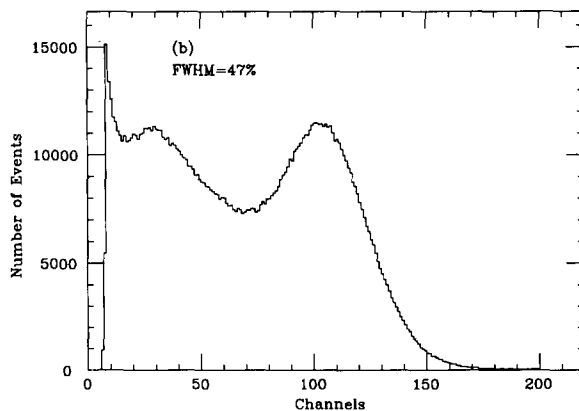
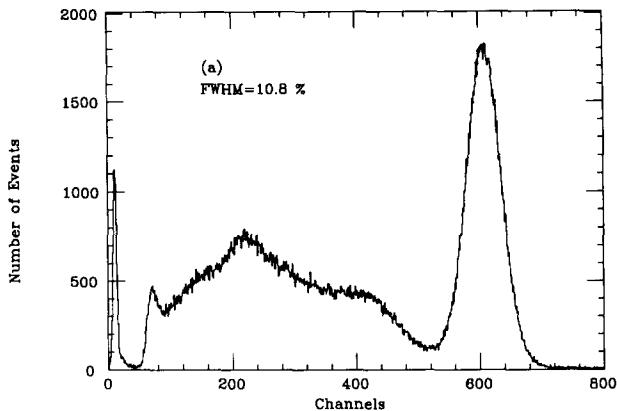


Fig. 3. BaF<sub>2</sub> pulse height spectrum with <sup>137</sup>Cs  $\gamma$ -rays with R1306 (a) and R3197 (b) phototubes.

An interactive program running on a Micro VAX II responded to a LAM (“look at me”) interrupt from the BGO FIFO module in the CAMAC crate. This program read out the BGO data from the FIFO module, and the integrated BaF<sub>2</sub> light pulse and the target beam charge

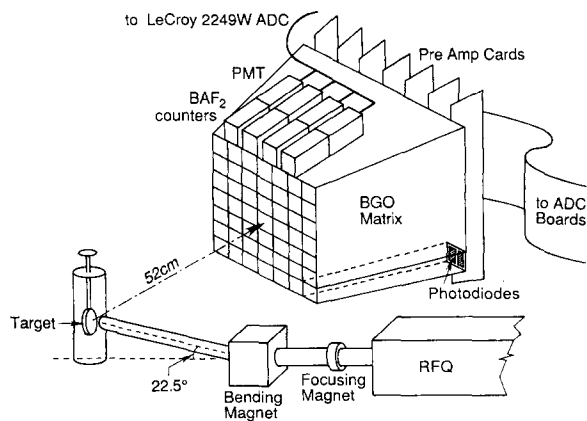


Fig. 4. AccSys test experimental setup.

Table 3  
Runs carried out at the 1988 AccSys test

Run no.	Target foil	Charge [ $\mu\text{C}/\text{pulse}$ ]	Comments
1–10	Punctured gold	0.11	
11–14	10 $\mu\text{m}$ Mo	0.13	
15	10 $\mu\text{m}$ Mo	0.13	Target shielded with 15 cm Cu
16–17	10 $\mu\text{m}$ Mo	0.13	Shielding removed
18	10 $\mu\text{m}$ Mo	0.12	Target shielded with 5 cm Al
19	10 $\mu\text{m}$ Mo	0.12	Target shielded with 5 cm Cu
20	10 $\mu\text{m}$ Mo	0.14	Shielding removed
21	10 $\mu\text{m}$ Mo	0.14	Target rotated by $10^\circ$
22–24	5 $\mu\text{m}$ Mo	0.14	Beam not stable
25	5 $\mu\text{m}$ Mo	0.132	Beam intensity was deliberately varied
26	5 $\mu\text{m}$ Mo	0.135	from run 25 to 28
27	5 $\mu\text{m}$ Mo	0.073	
28	5 $\mu\text{m}$ Mo	0.044	
35–44	5 $\mu\text{m}$ Mo	$\sim 0.035$	Mo collimator placed in front of target
45	5 $\mu\text{m}$ Mo	0.037	Charge on target was varied by adjusting the focus of the quadrupole magnets
46	5 $\mu\text{m}$ Mo	0.024	from run 45 to 49
47	5 $\mu\text{m}$ Mo	0.031	
48	5 $\mu\text{m}$ Mo	0.039	
49	5 $\mu\text{m}$ Mo	0.035	Large statistics run

from the LeCroy 2249W ADC module. Data were then written into a file on a hard disk for off-line analysis. For the BGO crystals, ADC values were converted to energy using the calibration constants obtained from the data analysis of the Li target runs. Temperature corrections were also made to the BGO ADC values.

Each run with a LiF target lasted for approximately 2 min, corresponding to approximately 3000 triggers. In order to demonstrate that precise calibrations can be achieved without RFQ beam stability during a run (although the RFQ pulses sometimes did reach 1.5% reproducibility over a run, even without any feedback controls), the beam current was varied during a special run series.

During another series of runs, materials were inserted between the target and the detector to study the beam properties, and to confirm that there was no significant neutron contamination of the photon flux produced from the target. Table 3 lists the runs taken, including the targets used and comments on the running conditions.

### 3. Results

#### 3.1. Photon pulse

Fig. 5 is a picture taken from an oscilloscope showing typical scintillation light pulses from two  $\text{BaF}_2$  counters. Fig. 5a shows the slow component, as measured with an R1306 PMT. Fig. 5b shows the fast component (along with a remainder of the slow component), as measured with an R2078 PMT. As shown in fig. 5a, a pulse-generator-like scintillation light pulse is obtained, because so many photons strike the crystal within the pulse. With the fast component, many individual spikes can be seen on the scope, but the integrated pulse area is quite well defined, with the spread of the distributions dominated by statistical fluctuations in the number of incident photons.

Although the RFQ pulse width used during the test was 8  $\mu\text{s}$ , a new pulse time-compressor at the output of their RFQ system will be developed by AccSys [9]. By using multiturn injection into and single-turn extraction from a small storage ring, up to 0.3  $\mu\text{C}$  charge could be

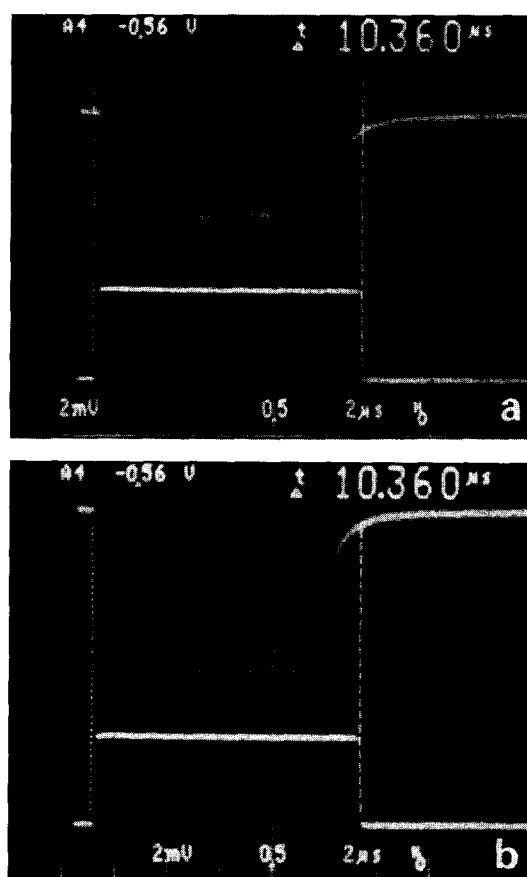


Fig. 5. Scintillation light pulse: slow (a) and fast (b) components.

compressed into a 100 ns or less beam pulse. This development will allow this technique to be used in calibrating calorimeters at the SSC and LHC.

3.2. Two normalization schemes

A precise normalization is needed to convert the integrated pulse read out for each crystal into a calibration constant. The energy deposited in each individual calorimeter element depends on the total number of protons striking the target on each beam pulse, the materials which the photon traverse before reaching a given calorimeter element, and the solid angle each calorimeter element subtends. The proton resonance spectrum resulting the decay of excited oxygen,  $^{16}\text{O}^*$ , is also complicated [5]. It is therefore difficult to calculate precisely the absolute energy deposited in each calorimeter element directly from a knowledge of the beam conditions and the geometrical setup.

However, within a run or within a series of runs with an identical geometrical arrangement, it is straightforward to obtain a precise relative calibration using this

technique. Apart from statistical fluctuations, the energy deposited in a calorimeter element only depends upon the number of protons hitting the target. A relative calibration constant can therefore be obtained by normalizing to (1) the total electric charge (proportional to the number of protons) collected from the target from each beam pulse, or (2) the response of a stable, external "standard" (i.e. a separate) counter or set of counters with high precision ADCs. We tested these two normalization schemes during the test. The BGO array was used as our external normalization standard.

To check the consistency of the two candidate normalization methods, we measured the total "beam charge" and the total energy deposited in the BGO matrix, and took their ratio for each beam pulse. Fig. 6a shows the measured beam charge distribution of run 27 without normalization. It is clear that the beam charge was not stable from pulse to pulse during the run: some deviations of up to 10% were observed. The distribution of beam charge, normalized to the total BGO energy is shown in fig. 6b. The almost perfect Gaussian distribution, with a 1.3% standard deviation, indicates that the two normalization schemes are consistent.

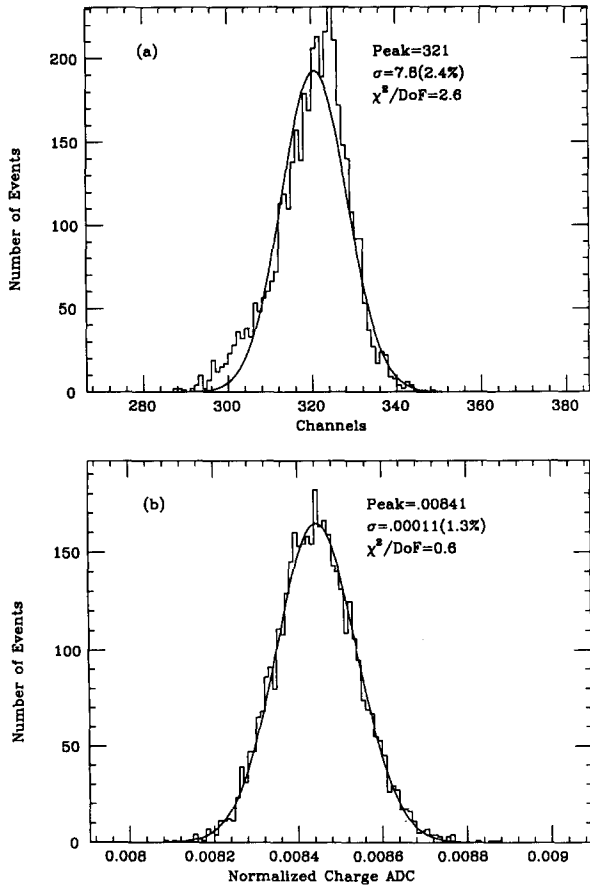


Fig. 6. The measured charge distribution of run 27 (a) and the distribution of charge normalized to the total BGO energy (b).

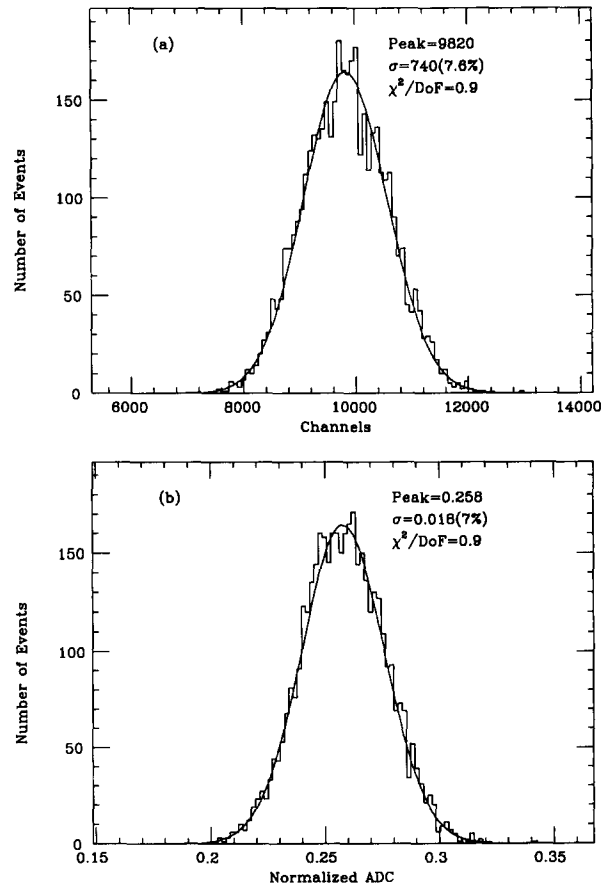


Fig. 7. ADC distribution of BGO crystal 25 without (a) and with (b) normalization to the total BGO energy for run 27.

Table 4  
Rms width (%) of detector response with and without normalization for run 25

Crystal	BGO26	BGO33	BaF1	BaF2	BaF3	BaF4	Beam
W/O norm	6.07	6.16	5.05	4.47	3.78	8.06	3.16
Norm. BGO	5.36	5.41	4.06	3.39	2.38	7.62	1.45
Norm. beam	5.54	5.55	4.09	3.39	2.49	7.65	N/A

Table 5  
Deviation of normalized peak positions (in %) for runs 45–49

Crystal	Run 45	Run 46	Run 47	Run 48	Run 49
BAF 1	0.32(8)	-0.00(8)	0.19(7)	0.06(6)	-0.57(3)
BAF 2	-0.31(6)	-0.36(6)	0.11(5)	0.53(5)	0.04(3)
BAF 3	-0.12(4)	-0.09(4)	0.14(4)	0.24(4)	-0.17(2)
BAF 4	0.62(14)	-0.19(15)	0.04(13)	-0.12(13)	-0.36(7)

rms = 0.29%

Normalizing the ADC distributions of the individual BGO and BaF<sub>2</sub> crystals, either to the beam charge or to the total BGO energy pulse by pulse, results in extremely clean Gaussian distributions. Fig. 7 shows the ADC distribution of a BGO crystal, number 25, before and after normalization to the BGO energy. Table 4 lists the rms widths in percent of the ADC distributions of some detector crystals with and without normalizations for run 25. The BGO energy normalization appears to be slightly better than the charge normalization, although the difference is not statistically significant.

### 3.3. Calibration stability

In order to check the stability of the calibration, using the two normalization schemes, the peak positions of the normalized ADCs were compared for a set of 5 runs with an identical setup but with different beam intensities.

Although the beam charge method works well within a run, it was found that the peaks of the normalized distributions for individual crystals showed significant shifts from run to run. The shifts were typically 2–3%, and sometimes more. This can be attributed to a change of the beam focus, or to slight changes in the position of the beam center relative to the active area of the target. As a result, the measured beam charge collected from the target holder is not always a precise measure of the number of protons hitting the active material in the target. Careful monitoring of beam focusing, and position, with feedback controls on the RFQ, and an improved target design are expected to help solve this problem. However, until we can demonstrate that target ageing will not affect the photon yield per unit of beam

charge over the long term, we have made the preliminary conclusion that the beam charge normalization method is not the best choice.

In contrast, the normalization to the BGO energy worked very well. Fig. 8 shows that the relative deviation of the peaks of individual BGO distributions from run to run, after normalization to the total BGO energy in the  $7 \times 7$  matrix, was Gaussian-distributed, with a standard deviation of 0.34%. Table 5 lists the relative deviation from run to run of the peaks for the BaF<sub>2</sub> crystals, normalized to the total BGO energy, where the numbers in bracket are statistical errors from fitting. The rms of the relative deviation is 0.29%. These deviations are dominated by statistical errors. It is therefore evident that a stability of better than 0.5% has been achieved with this normalization scheme.

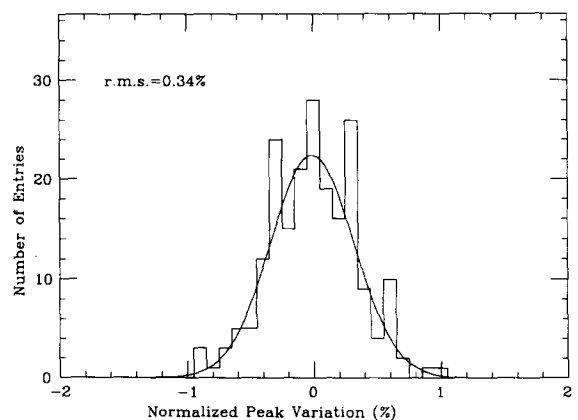


Fig. 8. Variation of the normalized peak positions from BGO crystals.

### 3.4. Correlation of calorimeter cells

The correlation of the normalized ADC values between any two individual BGO crystals was calculated. This correlation is defined as

$$\left( \sum_{i=1}^N x_i y_i / N - \sum_{i=1}^N x_i / N \times \sum_{i=1}^N y_i / N \right) / (\sigma_x \sigma_y), \quad (1)$$

where  $N$  is the total number of events in a run,  $x$ ,  $y$  are the normalized ADC values of the two crystals, and  $\sigma_x$ ,  $\sigma_y$  are their standard deviations.

It was found that the correlation is less than 0.05, which indicates that the values read out of individual crystals during a run can be considered as independent quantities. The resultant calibration constants obtained will therefore also have statistically independent errors.

### 3.5. Equivalent photon energy

As discussed in the last section, the energy of the protons hitting the fluoride crystal target were different for the three different targets. We measured the equivalent photon energy (EPE), defined as the sum of the energies of photons from one beam pulse hitting one crystal detector, and were thereby able to determine the photon yield per unit of beam charge on target, at three proton energies.

Table 6 lists the measured equivalent photon energies emitted into 1.6 msr (corresponding to a single L3 BGO crystal with a  $2 \times 2$  cm<sup>2</sup> front face at 50 cm from the target), per 0.1  $\mu$ C of beam charge on the target. The dependence of the photon energy on the proton energy is consistent with estimations from published resonance data [5]. The neutron background from the target with punctured gold did not contribute significantly to the energy measured because the proton beam energy was only 0.04 MeV above the neutron production threshold, and the detectors were in the backward hemisphere.

Table 6  
Equivalent photon energy emitted into 1.6 msr

Target foil	5 $\mu$ m Mo	10 $\mu$ m Mo	Punctured Au
Equiv. photon energy [GeV/0.1 $\mu$ C]	1.29	0.37	2.38

Table 7  
Relative photon yield from a LiF target

Proton energy [MeV]	1.2	1.6	1.9	2.5	2.9	3.2	3.5	3.85
Photon yield	0.4	1.0	2.0	12	22	27	29	32

During the AccSys test we typically used a beam pulse of 0.10–0.15  $\mu$ C. In order to adapt this technique for future hadron colliders, such as the SSC or LHC, however, the pulse length of several  $\mu$ s may not match the experimental readout electronics. As discussed in ref. [9], recent computer simulation studies at Saclay have shown that it should be possible to compress beam pulses of 0.1–0.3  $\mu$ C into 100 ns time or less, by using multiturn injection into – and single-turn extraction from – a small storage ring. The time structure of this kind of beam pulse is well within the range of readout speeds planned for calorimeters at the SSC and LHC. The existing RFQ (1.92 MeV) and a LiF target could therefore be used as these accelerators to provide short pulses up to 7 GeV equivalent on a bare crystal target, or 4 GeV equivalent for a target covered with a 5  $\mu$ m Mo foil (0.3  $\mu$ C charge).

There are, however, much stronger fluorine resonances between 2.0 and 4.0 MeV [5]. Table 7 lists the ratio of the expected photon yield from a thick LiF target, as a function of the incident proton beam energy, to the yield from a 1.6 MeV proton beam (corresponding to a 5  $\mu$ m Mo foil with the existing RFQ). A 29-fold increase in the equivalent photon energy is expected when a 3.5 MeV proton beam hits the LiF target. Using a 3.85 MeV RFQ with the 5  $\mu$ m Mo foil-covered LiF target, one could thus obtain an equivalent photon energy of more than 40 GeV/(0.1  $\mu$ C). Using a CaF<sub>2</sub> target, which is easier to handle than LiF and which would have no neutron production as a by-product below 4.05 MeV [5], an equivalent photon energy per calorimeter element of 20 GeV/(0.1  $\mu$ C) or more is expected.

### 3.6. Energy spectrum of individual photons

The width of the normalized ADC distribution and the total energy in a crystal are strongly correlated. Fig. 9 shows the normalized ADC distributions of BGO crystal number 32, for runs with different beam intensities. It is clear that the rms width increases as the total energy deposited in the crystal decreases.

Assuming that the shape of the energy spectrum for the individual photons emitted by the target does not change as a function of beam intensity, the width of the observed energy distribution should be a measure of the inverse of the square root of the average number of photons. In order to test this, we defined the “relative rms”,  $\sigma_R$ , as the ratio of the rms width divided by the

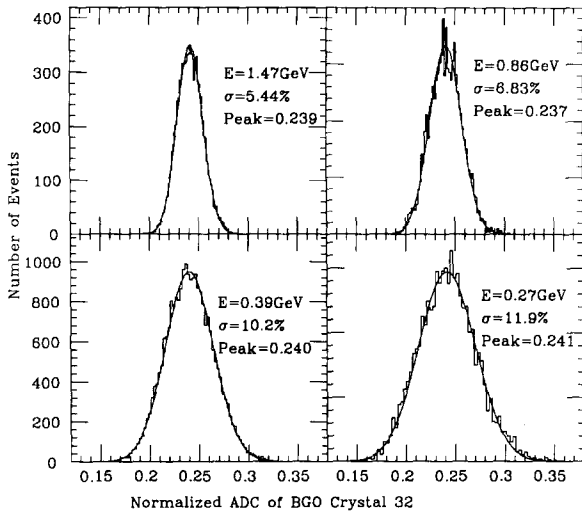


Fig. 9. Normalized ADC distribution of crystal 32 at different energies.

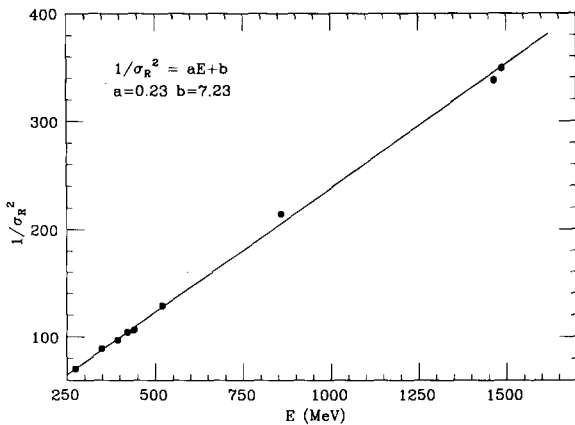


Fig. 10. Correlation between the relative rms and the average energy in BGO crystal 32.

energy corresponding to the peak (i.e. the average obtained with a Gaussian fit) of the distribution. Fig. 10 is a plot of  $(1/\sigma_R)^2$  versus the observed average photon energy for a BGO crystal, for a series of nine runs where the beam intensity varied by a factor of 6. The excellent linearity shown in the figure tends to confirm

Table 8

Average photon energy ( $EPE \times \sigma_R^2$ )

Run	25	26	27	28	45	46	47	48	49
$EPE_{32}$ [GeV]	1.47	1.49	0.86	0.52	0.42	0.27	0.35	0.44	0.39
Photon number	359	364	209	127	105	68	88	109	98
Measured $E_{ave}$ [MeV]	4.10	4.09	4.11	4.10	4.00	4.01	4.00	4.04	4.07

Average = 4.06 MeV, rms = 0.15 MeV

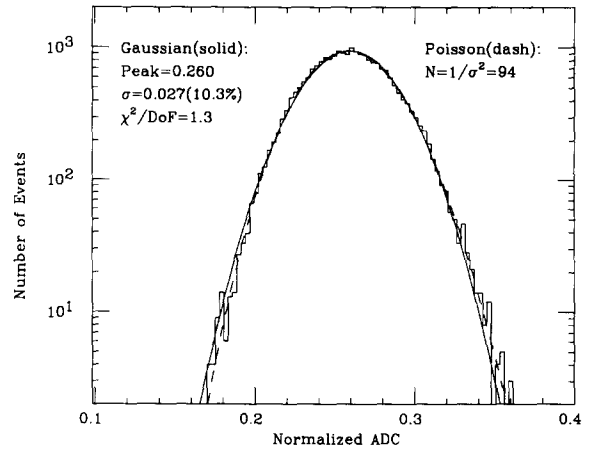


Fig. 11. A Gaussian fit compared with a Poisson fit for the normalized ADC of crystal 25 from run 49.

that the widths of the distributions are due to statistical fluctuations. The average number of photons hitting the target per pulse should therefore be given by  $1/(\sigma_R)^2$ .

The average energy of the photons emitted by the target can then be obtained by dividing the equivalent photon energy by the average number of photons. Table 8 shows the equivalent photon energy in crystal 32 ( $EPE_{32}$ ), and the energy of the individual photons averaged over all the BGO crystals ( $E_{ave}$ ), for nine different runs.

Bearing in mind that the predominant photons from  $^{16}O^*$  decay have an energy of 6.13 MeV, we estimated that the 4.1 MeV average energy was due to energy sharing between neighboring crystals, i.e. the equivalent photon number was increased. This estimation was confirmed by a series of EGS Monte Carlo simulations [10].

A constant  $E_{ave}$  indicates that the widths of the normalized ADC distributions are dominated by the statistical fluctuations in the number of photons detected by each crystal, and that the photon energy spectrum remains the same when the beam intensity is varied.

### 3.7. Gaussian vs Poisson-distributed spectra

When the average number of photons per pulse hitting a calorimeter cell is not very large, a Poisson

Table 9  
Attenuation of the calibration pulse by Al and brass absorbers

Run	Material	Beam [ch]	EPE <sub>ave</sub> [MeV]	Measured attenuation	Estimated attenuation
17	0	520	334		
18	2 in. Al	526	206	0.609 ± 0.006	0.65 ± 0.03
19	2 in. brass	537	100	0.290 ± 0.003	0.27 ± 0.02

distribution should describe the normalized spectrum better than a Gaussian one. Fig. 11 shows a semilogarithmic plot of the normalized ADC distribution of BGO crystal 25 for run 49, which had low intensity per pulse and high statistics. We fitted the distribution with a Gaussian, and compared the fit to the result of using a Poisson distribution with a mean energy matching the mean of the measured distribution. It should be emphasized that the Poisson distribution is not just a fit, but is completely determined by the methods summarized in the previous section. As expected, the Poisson distribution matches the data better. The quality of the match, and the fact that the distribution in fig. 11 has no tails down to the 0.1% level, indicates that the distribution is completely free of background.

For equivalent photon energies above a few GeV, the deviation of the data from a Gaussian distribution is negligible. In this case, the data can be fit with a simple Gaussian with systematic effects from the fit which are well below the 0.1% level.

### 3.8. Attenuation of the calibration pulse

In order to check the nature of the particles which are emitted by the target, several runs were taken with the 10  $\mu\text{m}$  Mo target, in which shielding materials of various types and thicknesses were placed between the target and the crystals. In this way, the attenuation of the particles could be tested, and the results could be compared to the attenuation expected for 6 MeV photons. Table 9 lists the measured beam charge, the average beam charge per pulse (in ADC channels, labeled "Beam"), and the equivalent photon energy averaged over all BGO crystals,  $E_{\text{ave}}$ , for runs with 2 in. Al and 2 in. brass absorbers. A run without additional attenuation is included for comparison. The measured attenuation factors shown in the table are corrected for the beam intensity.

The measured attenuation factors were compared with the estimated attenuation factors, which are also listed in the table. The estimated attenuation factors were obtained by using the mass attenuation coefficients of 6 MeV photons. The 5% errors in the estimated attenuation values are dominated by the errors in the absorber thickness, by the effects of the finite transverse dimensions of the absorber, and by the uncer-

tainty in the precise admixture of secondary metals in the aluminum and brass alloys used. The agreement between the measured and estimated attenuation factors indicates that the calibration beam pulse is indeed a photon pulse.

## 4. Summary and conclusions

A novel technique to produce a calibration pulse with equivalent photon energy of up to 20 GeV or more in a typical calorimeter element, using an RFQ accelerator, has been successfully tested. The photon pulse can be used to calibrate electromagnetic calorimeters at present and future high energy physics experiments. With proper normalization and an RFQ repetition rate of 30 Hz or more, an entire electromagnetic calorimeter with  $10^4$  elements can be calibrated in 1–2 min with an accuracy of 0.5% or better.

The technique described here could be used without modification to calibrate calorimeters at the present generation of accelerators (such as LEP and HERA) or at electron-positron colliders planned for the future in the TeV range (such as CLIC or the TLC). A precise, separately read out subarray, at a large angle to the colliding beams and with very precise ADCs, could be used as an external normalization "standard", which could be cross-checked against normalization according to the beam charge on the target, pulse by pulse.

A potentially very high energy equivalent photon pulse can be obtained with a  $\text{CaF}_2$  target by using a higher energy RFQ to take advantage of the large fluorine resonances above 2 MeV.  $\text{CaF}_2$  is a good target material because of its relative ease of handling and because there are no significant neutron resonances in Ca below 4.05 MeV. In calorimeters where such a large equivalent energy per pulse is not required, the use of a  $\text{CaF}_2$  can reduce the output current requirements in the RFQ design.

This method can also be adapted for use at the next generation of hadron colliders, such as the SSC or LHC. In order to make the RFQ-based technique practical at these future accelerators, the external standard subarray should be made of radiation resistant material, such as  $\text{BaF}_2$  crystals. (An array of this type is currently under development at Caltech, BNL and the Shanghai In-

stitute of Ceramics.) In order to match the readout electronics for an SSC or LHC calorimeter, a small storage ring at the output of the RFQ system may be required, to compress the pulse to 100 ns or less in length. As mentioned in this report, AccSys Technology, Inc. intends to develop this technology under a grant from the Small Business Innovation Research (SBIR) program of the US Department of Energy [9].

### Acknowledgements

We are grateful to Prof. F. Takasaki and to Merck, Inc. who lent us BaF<sub>2</sub> crystals. G Ludlam help prepare the BaF<sub>2</sub> crystals at Caltech before the AccSys test. The BGO crystals, photodiodes, preamps and parts of the readout electronics were provided to use by members of the L3 Collaboration, especially the Aachen, Annecy, Lyon and Princeton groups. We would also like to thank Profs. C. Barnes and R. Kavanagh for many useful discussions, and for providing us with the use of the Van de Graaff facility at the Kellogg Lab at Caltech. The assistance of S. Sondergaard, J. Hanson, M. Hamm and many members of the Caltech technical staff, and AccSys, Inc. is appreciated. The continued support and encouragement of Profs. S.C.C. Ting and A. Zichichi are also gratefully acknowledged.

### References

- [1] M.D.G. Gilchriese, Proc. 1984 Summer Study on the Design and Utilization of the Superconducting Super Collider, eds. R. Donaldson and J.G. Morfin, Snowmass, Co. (1984) p. 607;
- H.H. Williams, Proc. 1986 Summer Study on the Physics of the Superconducting Super Collider, eds. R. Donaldson and J. Marx, Snowmass, Co. (1986) p. 327;
- SSC Central Design Group, SSC-SR-1021 (1986).
- [2] D.E. Groom, Proc. 1988 Summer Study on the High Energy Physics in 1990's, Snowmass, Co. (1988).
- [3] T.Q. Zhou et al., Nucl. Instr. and Meth. 258 (1987) 58; R.Y. Zhu, EGS Study of BGO Calibration Using Low Energy Photons, L3 Internal report (December, 1985); H. Newman and R.Y. Zhu, Proposal for a BGO Calibration Test at AccSys (October, 1987).
- [4] H. Ma et al., Nucl. Instr. and Meth. A274 (1989) 113.
- [5] F. Ajzenberg-Selove, Nucl. Phys. A475 (1987) 1; H.B. Willard et al., Phys. Rev. 85 (1952) 849.
- [6] M. Lavel et al., Nucl. Instr. and Meth. A206 (1983) 169; P. Schotanus et al., Nucl. Instr. and Meth. A259 (1987) 586 and IEEE Trans. Nucl. Sci. NS-34 (1987) 76.
- [7] S. Majewski and D. Anderson et al., Nucl. Instr. and Meth. A241 (1985) 76; A.J. Caffrey et al., IEEE Trans. Nucl. Sci. NS-33 (1986) 230; S. Majewski et al., Nucl. Instr. and Meth. A260 (1987) 373.
- [8] L3 Collaboration, L3 Technical Proposal (May, 1983); J. Bakken et al., Nucl. Instr. and Meth. A254 (1987) 535 and A228 (1985) 294.
- [9] R. Hamm, SSC Electromagnetic Calorimeter Calibration Source, Phase II proposal to the DoE SBIR program (December, 1988).
- [10] Electron Gamma Shower (EGS) program by R. Ford and W. Nelson. See Report SLAC-210 (1978).

- [1] M.D.G. Gilchriese, Proc. 1984 Summer Study on the Design and Utilization of the Superconducting Super